

An extended study of the prompt photon photoproduction at HERA with k_T -factorization

A.V. Lipatov, M.A. Malyshev, N.P. Zotov

February 17, 2019

*D.V. Skobeltsyn Institute of Nuclear Physics,
M.V. Lomonosov Moscow State University,
119991 Moscow, Russia*

Abstract

We reconsider the prompt photon photoproduction at HERA in the framework of the k_T -factorization QCD approach. The proposed method is based on the $\mathcal{O}(\alpha^2\alpha_s)$ amplitudes for $\gamma q \rightarrow \gamma g q$ and $\gamma g^* \rightarrow \gamma q \bar{q}$ partonic subprocesses. Additionally, we take into account the $\mathcal{O}(\alpha^2\alpha_s^2)$ box contributions $\gamma g \rightarrow \gamma g$ to the production cross sections. The unintegrated (or transverse momentum dependent) parton densities in the proton are determined using Kimber-Martin-Ryskin (KMR) prescription. Our consideration covers both inclusive and jet associated prompt photon photoproduction rates. We find that our numerical predictions agree well with the recent data taken by H1 and ZEUS collaborations at HERA. We demonstrate that the box contributions are sizeable and amount up to $\sim 15\%$ of the calculated total cross section.

1 Introduction

The prompt (or direct) photon production¹ at high energies is an important tool to study the hard subprocess dynamics, since the resulting photons are largely insensitive to the effects of the final state hadronization. It is a subject of a special interest since, in particular, measurements of total and differential cross sections of prompt photons can be used to constrain the parton densities in a proton. In the electron-proton collisions at HERA, the ZEUS and H1 Collaborations previously reported the data [1–4] on the production of prompt photons in photoproduction events, where the virtuality of the exchanged photon Q^2 is lower than 1 GeV². The next-to-leading order (NLO) pQCD calculations [5–7] underestimate these data

¹Usually the photons are called 'prompt' if they are coupled to the interacting quarks.

by 30—40%, especially in rear pseudo-rapidity (electron direction) region, and observed disagreement is difficult to explain with conventional theoretical uncertainties connected with scale dependence and parametrizations of the parton densities [3,4]. However, as it was pointed out in [3,4], the HERA data can be reasonably well described by the calculations [8,9] performed in the framework of the k_T -factorization QCD approach [10–13], which is based on the famous Balitsky-Fadin-Kuraev-Lipatov (BFKL) [14,15] dynamics of parton evolution².

Very recently new preliminary results for prompt photon photoproduction cross sections (both inclusive and associated with the hadronic jet) have been reported [17] by the ZEUS Collaboration. In the present note we apply the k_T -factorization approach of QCD for the analyses of these data. Note that our previous consideration [8,9] was based on the off-shell $\mathcal{O}(\alpha^2)$ partonic amplitudes for direct ($\gamma q^* \rightarrow \gamma q$) and resolved photon ($q^* g^* \rightarrow \gamma q$, $g^* q^* \rightarrow \gamma q$ and $q^* \bar{q}^* \rightarrow \gamma g$) contributions to the photon cross section, where the non-zero transverse momenta of initial quarks and gluons were properly taken into account. Here we reconsider our previous calculations and take into account $\mathcal{O}(\alpha^2 \alpha_s)$ subprocesses, namely $\gamma g^* \rightarrow \gamma q \bar{q}$ and $\gamma q \rightarrow \gamma g q$. In the case of photon and associated jet production, it allows us to take into account the kinematics of the accompanied jet more accurately as compared with the previous consideration (see discussion in Section 3). Additional motivation of our study is that similar consideration [18], based on the off-shell $2 \rightarrow 3$ subprocesses, results in a better description of the Tevatron data on the associated photon and heavy (b or c) quark jet [19,20] as compared to the NLO pQCD predictions [21]. Moreover, we take into account $\mathcal{O}(\alpha^2 \alpha_s^2)$ contributions from the box $\gamma g \rightarrow \gamma g$ subprocess³, which is known to be sizeable [7] since the high gluon density region is partially reached. Following to our previous considerations [8,9], we apply Kimber-Martin-Ryskin (KMR) prescription [22,23] to define the unintegrated (or transverse momentum dependent) quark and gluon densities in a proton. This approach is a simple formalism to construct the unintegrated parton distributions from the known collinear ones. We calculate total and differential inclusive and jet associated prompt photon production cross sections, perform a systematic comparison of our predictions with the available H1 and ZEUS data [4,17] and estimate the theoretical uncertainties of our predictions.

The outline of our paper is following. In Section 2 we recall shortly the basic formulas of the k_T -factorization approach. In Section 3 we present the numerical results of our calculations and discussion. Section 4 contains our conclusions.

2 Theoretical framework

The previous investigation [8,9] in the framework of the k_T -factorization approach was based on $\mathcal{O}(\alpha^2)$ off-shell subprocesses, namely

$$\gamma(k_1) + q^*(k_2) \rightarrow \gamma(p_1) + q(p_2), \quad (1)$$

$$q^*(k_1) + \bar{q}^*(k_2) \rightarrow \gamma(p_1) + g(p_2), \quad (2)$$

$$q^*(k_1) + g^*(k_2) \rightarrow \gamma(p_1) + q(p_2), \quad (3)$$

$$g^*(k_1) + q^*(k_2) \rightarrow \gamma(p_1) + q(p_2), \quad (4)$$

where the subprocess (1) represents the direct production mechanism, and the subprocesses (2) — (4) represent the single resolved photon ones, in which the initial photon fluctuated

²See, for example, reviews [16] for introduction to the k_T -factorization formalism.

³We will neglect the transverse momenta of incoming quarks and gluons in the production amplitudes of $\gamma q \rightarrow \gamma g q$ and $\gamma g \rightarrow \gamma g$ subprocesses, but keep true off-shell kinematics. See Section 2 for more details.

into a hadronic state and a gluon and/or a quark from this hadronic fluctuation takes part in the hard interaction⁴. In the present note we concentrate on $\mathcal{O}(\alpha^2\alpha_s)$ subprocesses:

$$\gamma(k_1) + q(k_2) \rightarrow \gamma(p_1) + g(p_2) + q(p_3), \quad (5)$$

$$\gamma(k_1) + g^*(k_2) \rightarrow \gamma(p_1) + q(p_2) + \bar{q}(p_3), \quad (6)$$

where the relevant four-momenta are given in the parentheses. Additionally, for the first time in the framework of k_T -factorization, we take into account box contribution:

$$\gamma(k_1) + g(k_2) \rightarrow \gamma(p_1) + g(p_2). \quad (7)$$

This subprocess, formally is of $\mathcal{O}(\alpha^2\alpha_s^2)$, is known to be sizeable [7] due to high gluon luminosity in the probed kinematical region and it was taken into account in the standard QCD calculations [6]. The corresponding Feynman diagrams for subprocesses under consideration are shown on Figs. 1 and 2. Note that, in contrast with the collinear QCD approximation, the subprocesses (1) — (3) are effectively included in (5) and (6) in the k_T -factorization approach, and only subprocess (4) stays out. However, according to the estimates [8], this mechanism gives only a few percent contribution to the cross section in the kinematical region covered by the H1 and ZEUS experiments, so we neglect it. We neglect also the contributions from the so-called fragmentation mechanisms since the applying of the isolation cuts [4,17] reduces these contributions to less than 10% of the visible cross section. Note that the isolation cuts and additional conditions which preserve our calculations from divergences were specially discussed in [9].

The off-shell amplitudes for the subprocesses (5) and (6) can be written as follows:

$$\mathcal{M}(\gamma q \rightarrow \gamma g q) = e^2 e_q^2 g t^a \epsilon_\lambda(k_1) \epsilon_\mu^*(p_1) \epsilon_\nu^*(p_2) \sum_{i=1}^6 \mathcal{F}_i^{\mu\nu\lambda}, \quad (8)$$

$$\mathcal{M}(\gamma g^* \rightarrow \gamma q \bar{q}) = e^2 e_q^2 g t^a \epsilon_\mu(k_1) \epsilon_\nu(k_2) \epsilon_\lambda^*(p_1) \sum_{i=1}^6 \mathcal{G}_i^{\mu\nu\lambda}, \quad (9)$$

where

$$\mathcal{F}_1^{\mu\nu\lambda} = \bar{u}(p_3) \gamma^\nu \frac{\hat{p}_2 + \hat{p}_3 + m}{(p_2 + p_3)^2 - m^2} \gamma^\mu \frac{\hat{k}_1 + \hat{k}_2 + m}{(k_1 + k_2)^2 - m^2} \gamma^\lambda u(k_2), \quad (10)$$

$$\mathcal{F}_2^{\mu\nu\lambda} = \bar{u}(p_3) \gamma^\mu \frac{\hat{p}_1 + \hat{p}_3 + m}{(p_1 + p_3)^2 - m^2} \gamma^\nu \frac{\hat{k}_1 + \hat{k}_2 + m}{(k_1 + k_2)^2 - m^2} \gamma^\lambda u(k_2), \quad (11)$$

$$\mathcal{F}_3^{\mu\nu\lambda} (= \bar{u}(p_3) \gamma^\nu \frac{\hat{p}_2 + \hat{p}_3 + m}{(p_2 + p_3)^2 - m^2} \gamma^\lambda \frac{\hat{k}_2 - \hat{p}_1 + m}{(k_2 - p_1)^2 - m^2} \gamma^\mu u(k_2), \quad (12)$$

$$\mathcal{F}_4^{\mu\nu\lambda} = \bar{u}(p_3) \gamma^\lambda \frac{\hat{p}_3 - \hat{k}_1 + m}{(p_3 - k_1)^2 - m^2} \gamma^\mu \frac{\hat{k}_2 - \hat{p}_2 + m}{(k_2 - p_2)^2 - m^2} \gamma^\nu u(k_2), \quad (13)$$

$$\mathcal{F}_5^{\mu\nu\lambda} (= \bar{u}(p_3) \gamma^\mu \frac{\hat{p}_1 + \hat{p}_3 + m}{(p_1 + p_3)^2 - m^2} \gamma^\lambda \frac{\hat{k}_2 - \hat{p}_2 + m}{(k_2 - p_2)^2 - m^2} \gamma^\nu u(k_2), \quad (14)$$

$$\mathcal{F}_6^{\mu\nu\lambda} = \bar{u}(p_3) \gamma^\lambda \frac{\hat{p}_3 - \hat{k}_1 + m}{(p_3 - k_1)^2 - m^2} \gamma^\nu \frac{\hat{k}_2 - \hat{p}_3 + m}{(k_2 - p_3)^2 - m^2} \gamma^\mu u(k_2), \quad (15)$$

⁴The subprocesses (2) — (4), which are formally of $\mathcal{O}(\alpha\alpha_s)$, give also the $\mathcal{O}(\alpha^2)$ contributions since the parton densities in a photon at leading-order have a behavior proportional to $\alpha \ln \mu^2 / \Lambda_{\text{QCD}}^2 \sim \alpha / \alpha_s$.

and

$$\mathcal{G}_1^{\mu\nu\lambda} = \bar{u}(p_2)\gamma^\lambda \frac{\hat{p}_2 - \hat{p}_1 + m}{(p_2 - p_1)^2 - m^2} \gamma^\mu \frac{\hat{k}_2 - \hat{p}_3 + m}{(k_2 - p_3)^2 - m^2} \gamma^\nu u(p_3), \quad (16)$$

$$\mathcal{G}_2^{\mu\nu\lambda} = \bar{u}(p_2)\gamma^\mu \frac{\hat{p}_2 - \hat{k}_1 + m}{(p_2 - k_1)^2 - m^2} \gamma^\lambda \frac{\hat{k}_2 - \hat{p}_3 + m}{(k_2 - p_3)^2 - m^2} \gamma^\nu u(p_3), \quad (17)$$

$$\mathcal{G}_3^{\mu\nu\lambda} = \bar{u}(p_2)\gamma^\mu \frac{\hat{k}_1 - \hat{p}_2 - m}{(k_1 - p_2)^2 - m^2} \gamma^\nu \frac{\hat{p}_3 + \hat{p}_1 - m}{(p_3 + p_1)^2 - m^2} \gamma^\lambda u(p_3), \quad (18)$$

$$\mathcal{G}_4^{\mu\nu\lambda} = \bar{u}(p_2)\gamma^\lambda \frac{\hat{p}_2 - \hat{p}_1 + m}{(p_2 - p_1)^2 - m^2} \gamma^\nu \frac{\hat{k}_1 - \hat{p}_3 + m}{(k_1 - p_3)^2 - m^2} \gamma^\mu u(p_3), \quad (19)$$

$$\mathcal{G}_5^{\mu\nu\lambda} = \bar{u}(p_2)\gamma^\nu \frac{\hat{p}_2 - \hat{k}_2 + m}{(p_2 - k_2)^2 - m^2} \gamma^\lambda \frac{\hat{k}_1 - \hat{p}_3 + m}{(k_1 - p_3)^2 - m^2} \gamma^\mu u(p_3), \quad (20)$$

$$\mathcal{G}_6^{\mu\nu\lambda} = \bar{u}(p_2)\gamma^\nu \frac{\hat{k}_2 - \hat{p}_2 - m}{(k_2 - p_2)^2 - m^2} \gamma^\mu \frac{\hat{p}_3 + \hat{p}_1 - m}{(p_3 + p_1)^2 - m^2} \gamma^\lambda u(p_3). \quad (21)$$

Here e is the electric charge, e_q is the (fractional) charge of quark having mass m , g is the strong charge, $\epsilon(k_1)$, $\epsilon(k_2)$, $\epsilon(p_1)$ and $\epsilon(p_2)$ are the polarization four-vectors of the corresponding particles and a is the eight-fold color index. Note that in (8) we neglected the transverse momentum of initial quark. Further calculation of the off-shell matrix elements listed above is a very straightforward. Here we would like to only mention that, according to the k_T -factorization prescription [11–14], the summation over the incoming off-shell gluon polarizations is carried out with

$$\sum \epsilon^\mu \epsilon^{*\nu} = \frac{k_T^\mu k_T^\nu}{\mathbf{k}_T^2}, \quad (22)$$

where k_T is the gluon non-zero transverse momentum. For the photons and outgoing on-shell gluon the summation over their polarizations can be performed with the usual covariant formula:

$$\sum \epsilon^\mu \epsilon^{*\nu} = -g^{\mu\nu}. \quad (23)$$

In other respects we follow the standard QCD Feynman rules. The evaluation of emerging traces was done using the algebraic manipulation system FORM [24]. Finally, concerning the box contribution (7), the corresponding amplitude squared was calculated a long time ago in the on-shell limit $\mathbf{k}_{2T}^2 \rightarrow 0$. The simple analytical expression can be found, for example, in [25]. In our phenomenological study, we apply this expression with one remark: numerically, we keep the exact off-shell kinematics (see [26] for more details).

According to the k_T -factorization prescription, to calculate the cross section one should convolute off-shell partonic cross sections with the relevant unintegrated (transverse momentum dependent) quark and/or gluon distributions in a proton. In the present paper we use the KMR approximation [22, 23] to determine it. The KMR approach is a formalism to construct the unintegrated parton densities $f_a(x, \mathbf{k}_T^2, \mu^2)$ from the known collinear parton distributions $xa(x, \mu^2)$, where $a = g$ or $a = q$. In this approximation, the unintegrated quark

and gluon densities are given by [22, 23]

$$f_q(x, \mathbf{k}_T^2, \mu^2) = T_q(\mathbf{k}_T^2, \mu^2) \frac{\alpha_s(\mathbf{k}_T^2)}{2\pi} \times \int_x^1 dz \left[P_{qq}(z) \frac{x}{z} q\left(\frac{x}{z}, \mathbf{k}_T^2\right) \Theta(\Delta - z) + P_{qg}(z) \frac{x}{z} g\left(\frac{x}{z}, \mathbf{k}_T^2\right) \right], \quad (24)$$

$$f_g(x, \mathbf{k}_T^2, \mu^2) = T_g(\mathbf{k}_T^2, \mu^2) \frac{\alpha_s(\mathbf{k}_T^2)}{2\pi} \times \int_x^1 dz \left[\sum_q P_{gq}(z) \frac{x}{z} q\left(\frac{x}{z}, \mathbf{k}_T^2\right) + P_{gg}(z) \frac{x}{z} g\left(\frac{x}{z}, \mathbf{k}_T^2\right) \Theta(\Delta - z) \right], \quad (25)$$

where $P_{ab}(z)$ are the usual unregulated LO DGLAP splitting functions. The theta functions which appear in (24) and (25) imply the angular-ordering constraint $\Delta = \mu/(\mu + |\mathbf{k}_T|)$ specifically to the last evolution step to regulate the soft gluon singularities. For other evolution steps, the strong ordering in transverse momentum within the DGLAP equations automatically ensures angular ordering⁵. The Sudakov form factors $T_q(\mathbf{k}_T^2, \mu^2)$ and $T_g(\mathbf{k}_T^2, \mu^2)$ which appear in (24) and (25) enable us to include logarithmic loop corrections to the calculated cross sections.

The contributions to the prompt photon cross sections from subprocesses (5) — (7) can be easily written as follows:

$$\sigma(\gamma p \rightarrow \gamma X) = \sum_q \int \frac{E_T^\gamma}{128\pi^3 y(x_2 s)^2} \overline{|\mathcal{M}(\gamma q \rightarrow \gamma qg)|^2} f_q(x_2, \mathbf{k}_{2T}^2, \mu^2) \times \times dy_1 dy_2 dy^\gamma dE_T^\gamma d\mathbf{k}_{2T}^2 \frac{d\phi_2}{2\pi} \frac{d\psi_1}{2\pi} \frac{d\psi_2}{2\pi} \frac{d\psi^\gamma}{2\pi}, \quad (26)$$

$$\sigma(\gamma p \rightarrow \gamma X) = \int \frac{E_T^\gamma}{128\pi^3 y(x_2 s)^2} \overline{|\mathcal{M}(\gamma g^* \rightarrow \gamma qg)|^2} f_g(x_2, \mathbf{k}_{2T}^2, \mu^2) \times \times dy_1 dy_2 dy^\gamma dE_T^\gamma d\mathbf{k}_{2T}^2 \frac{d\phi_2}{2\pi} \frac{d\psi_1}{2\pi} \frac{d\psi_2}{2\pi} \frac{d\psi^\gamma}{2\pi}, \quad (27)$$

$$\sigma(\gamma p \rightarrow \gamma X) = \int \frac{E_T^\gamma}{8\pi y(x_2 s)^2} \overline{|\mathcal{M}(\gamma g \rightarrow \gamma g)|^2} f_g(x_2, \mathbf{k}_{2T}^2, \mu^2) \times \times dy^\gamma dE_T^\gamma d\mathbf{k}_{2T}^2 \frac{d\phi_2}{2\pi} \frac{d\psi^\gamma}{2\pi}, \quad (28)$$

where s is the total center-of-mass energy of the collision, ϕ_2 is the azimuthal angle⁶ of initial quark or gluon having fraction x_2 of the initial proton longitudinal momentum and non-zero transverse momentum $|\mathbf{k}_{2T}| \neq 0$, E_T^γ , y^γ , ϕ^γ are the transverse energy, rapidity and azimuthal angle of the produced photon, y_1 , y_2 , ψ_1 and ψ_2 are the rapidities and azimuthal angles of the outgoing partons, respectively.

The experimental data [4, 17] refer to the prompt photon production in ep collisions, where the electron emits a quasi-real ($Q^2 \sim 0$) photon. Thus γp cross sections (26) — (28) should be weighted with the photon flux in the electron:

$$d\sigma(ep \rightarrow e' + \gamma + X) = \int f_{\gamma/e}(y) d\sigma(\gamma p \rightarrow \gamma + X) dy, \quad (29)$$

⁵Numerically, in (24) and (25) we applied the MSTW'2008 parton distributions [27].

⁶The angle of the transverse momentum \mathbf{k}_T in the plane perpendicular to OZ axis.

where y is the fraction of the initial electron energy carried by the photon in the laboratory frame. We use here the Weizacker-Williams approximation for the bremsstrahlung photon distribution from the electron:

$$f_{\gamma/e}(y) = \frac{\alpha}{2\pi} \left(\frac{1 + (1-y)^2}{y} \ln \frac{Q_{\max}^2}{Q_{\min}^2} + 2m_e^2 y \left(\frac{1}{Q_{\max}^2} - \frac{1}{Q_{\min}^2} \right) \right), \quad (30)$$

where m_e is the electron mass, $Q_{\min}^2 = m_e^2 y^2 / (1-y)^2$ and $Q_{\max}^2 = 1 \text{ GeV}^2$, which is a typical value for the recent photoproduction measurements at the HERA collider.

The multidimensional integration in (26) — (28) has been performed by means of the Monte-Carlo technique, using the routine VEGAS [28]. The full C++ code is available from the authors on request⁷.

3 Numerical results

Now we are in a position to present our numerical results. First we describe our theoretical input and the kinematical conditions. The renormalization and factorization scales were taken as $\mu_R = \mu_F = \xi E_T^\gamma$, where the parameter ξ was varied between 1/2 and 2 about the default value $\xi = 1$ to estimate the scale uncertainties of our calculations. We neglected quark masses and used the standard LO formula for the strong coupling constant $\alpha_s(\mu^2)$ with $n_f = 4$ massless quark flavours and $\Lambda_{\text{QCD}} = 200 \text{ MeV}$, such that $\alpha_s(M_Z^2) = 0.1232$.

The experimental data for the inclusive prompt photon photoproduction at HERA were taken by both the H1 and ZEUS collaborations. The H1 data [4] were obtained in the following kinematical region⁸: $6 < E_T^\gamma < 15 \text{ GeV}$ and $-1.0 < \eta^\gamma < 2.4$. The fraction y of the electron energy transferred to the photon is restricted to the range $0.1 < y < 0.7$. Very recent ZEUS measurements [17] refer to the region defined by $6 < E_T^\gamma < 15 \text{ GeV}$, $-0.7 < \eta^\gamma < 0.9$ and $0.2 < y < 0.7$. In the case of jet associated prompt photon photoproduction the restrictions on the prompt photon transverse momentum and pseudo-rapidity are the same as in the inclusive production case. For the jets, the cuts which were applied in the H1 and ZEUS analyses are $E_T^{\text{jet}} > 4.5 \text{ GeV}$, $-1.3 < \eta^{\text{jet}} < 2.3$ and $4 < E_T^{\text{jet}} < 35 \text{ GeV}$ and $-1.5 < \eta^{\text{jet}} < 1.8$, respectively. The data [4, 17] were obtained with the electron energy $E_e = 27.6 \text{ GeV}$ and the proton energy $E_p = 920 \text{ GeV}$.

The transverse energy and pseudo-rapidity distributions of the inclusive prompt photon production are shown in Figs. 3 — 4 in comparison with the H1 and ZEUS data [4, 17]. In the left panels, the solid histograms correspond to the predictions obtained from (26) — (28) at the default scale. The dashed histograms represent the corresponding theoretical uncertainties estimated as it was described above. We find that our predictions reasonably well describe a full set of the available experimental data. Moreover, the shape and absolute normalization of the measured cross sections are adequately reproduced within the theoretical and experimental uncertainties. Additionally we plot predictions based on the $2 \rightarrow 2$ subprocesses (1) — (4), as it was done in our previous paper [8, 9] (dotted histograms in the left panels)⁹. One can see some enhancement of the calculated cross sections due to,

⁷malyshev@theory.sinp.msu.ru

⁸Here and in the following all kinematic quantities are given in the laboratory frame with positive OZ axis direction given by the proton beam.

⁹The depicted $2 \rightarrow 2$ subprocesses based results differ a little from the ones presented in [8, 9], since the former have been obtained with the MSTW parton distributions instead of older GRV94 set as the input for KMR.

in particular, the box subprocess (7) included into our present consideration. The relative contributions of different subprocesses to the prompt photon cross section are shown on the right panels of Figs. 3 — 4. We find that while the subprocess (5) dominates, the box subprocess (7) contributes significantly to the predicted cross section, specially at negative photon pseudorapidities. In this region, the box contribution is comparable with the contribution from the subprocess (6), and it amounts up to $\sim 15\%$ of the total cross section of inclusive prompt photon production.

Now we turn to the prompt photon production associated with the hadronic jet. In the previous consideration [8, 9], to calculate the semi-inclusive production rates some approximation was applied. So, it was noted that the produced photon is accompanied by a number of partons radiated in the course of the parton evolution. On the average, the parton transverse momentum decreases from the hard interaction box towards the proton. As an approximation, it was assumed that the parton k' , emitted in the last evolution step, compensates the whole transverse momentum of the parton participating in the hard subprocess, i.e. $\mathbf{k}'_T \simeq -\mathbf{k}_T$. All the other emitted partons are collected together in the proton remnant, which is assumed to carry only a negligible transverse momentum compared to \mathbf{k}'_T . This parton gives rise to a final hadron jet with $E_T^{\text{jet}} = |\mathbf{k}'_T|$ in addition to the jet produced in the hard subprocess. From these hadron jets the one carrying the largest transverse energy has been choosed [8, 9]. In the present paper we use the same approximation. However, since we use $2 \rightarrow 3$ rather than $2 \rightarrow 2$ subprocesses, the jet production kinematics is described more accurately than it was done previously, because of the production of jets mainly from the hard subprocesses.

Our numerical predictions are shown in Figs. 5 — 8 (on the left panels) in comparison with the H1 and ZEUS data [4, 17]. The relative contributions of different subprocesses are shown in the right panels. One can see that the situation is very similar to the inclusive production case. The reasonably good description of the data for a number of measured distributions is achieved except for the distributions on the η^{jet} , where some disagreement in the shape takes place. The same shape disagreement in the η^{jet} distributions is observed in the predictions based on the $2 \rightarrow 2$ subprocesses (1) — (4). Therefore we can conclude that the possible reason of such discrepancy can be connected with the approximation for the jet determination which was described above and which was used in both type of calculations. Note that the predictions based on the former scheme give the results tending to underestimate the data, while the approach based on the $2 \rightarrow 3$ subprocesses (5) — (7) shows a better agreement. We find that the box contribution (7) is important in the photon and jet associated production case also. One can see that its contribution is comparable with the $\gamma q \rightarrow \gamma qg$ subprocess.

Other important variables in prompt photon photoproduction investigations are the longitudinal momenta of the partons in the colliding particles. The momentum fraction of the initial photon is introduced in the ZEUS analyses [17] as the following:

$$x_\gamma^{\text{obs}} = \frac{E_T^\gamma e^{-\eta^\gamma} + E_T^{\text{jet}} e^{-\eta^{\text{jet}}}}{2yE_e}. \quad (31)$$

At $x_\gamma^{\text{obs}} > 0.85$ the cross section is dominated by the direct initial photons contributions, whereas at lower x_γ^{obs} the resolved photon contributions dominate. The H1 collaboration refers to x_γ^{LO} and x_p^{LO} observables [4] given by:

$$x_\gamma^{\text{LO}} = \frac{E_T^\gamma (e^{-\eta^\gamma} + e^{-\eta^{\text{jet}}})}{2yE_e}, \quad x_p^{\text{LO}} = \frac{E_T^\gamma (e^{-\eta^\gamma} + e^{-\eta^{\text{jet}}})}{2E_p}. \quad (32)$$

It was shown [4] that these quantities make explicit use only of the proton energy, which is better measured than the jet energy. Our predictions for these observables are shown in Figs. 9 — 10 in comparison with the H1 and ZEUS data. We demonstrate that, in the framework of k_T -factorization, the subprocesses (5) and (6) allow us to take into account both direct and resolved contributions without introducing any parton densities in a photon. So, one can see that while the direct region with $x_\gamma^{\text{obs}} > 0.85$ is dominated by the subprocess (5), which incorporates the contribution from the subprocess (1). In the resolved photon region, where $x_\gamma^{\text{obs}} < 0.85$, the contribution of the subprocess (6) becomes more important, since it contains the single resolved photon contribution (3). We point out that the approach based on the $2 \rightarrow 3$ subprocesses (5) — (7) shows a better agreement with the data at intermediate $0.6 < x_\gamma^{\text{obs}} < 0.9$ compared with the approach based on the $2 \rightarrow 2$ subprocesses (1) — (4). This is a result of more accurate treatment of jet production kinematics achieved in a presented approach.

4 Conclusion

We have reconsidered the inclusive and jet associated prompt photon photoproduction at HERA in the framework of k_T -factorization QCD formalism. The proposed approach has been based on the $\mathcal{O}(\alpha^2\alpha_s)$ off-shell amplitudes for $\gamma q \rightarrow \gamma g q$ and $\gamma g^* \rightarrow \gamma q \bar{q}$ partonic subprocesses. Similar consideration had a success in the description of the Tevatron data on the associated photon and heavy quark jet taken by the D0 and CDF collaborations [19, 20]. We have taken into account also the $\mathcal{O}(\alpha^2\alpha_s^2)$ box contributions $\gamma g \rightarrow \gamma g$ to the production cross sections. The unintegrated (or transverse momentum dependent) parton densities in the proton have been determined using Kimber-Martin-Ryskin (KMR) prescription. We have demonstrated that the proposed approach results in the better agreement with the HERA data in contrast with the previous k_T -factorization predictions based on the $2 \rightarrow 2$ subprocesses. We find that the box contributions are sizeable and amount up to $\sim 15\%$ of the calculated total cross section. It is important for the further theoretical and experimental investigations of prompt photon production associated with the hadronic jet(s) at the LHC energies.

Acknowledgements

We would like to thank P. Bussey, A. Iudin and I. Skillicorn for a useful discussion on the experimental data and the obtained results. This research was supported in part by the FASI of Russian Federation (grant NS-3920.2012.2), RFBR grants 12-02-31030 and 13-02-01060 and the grant of the Ministry of education and sciences of Russia (agreement 8412). A.L. and N.Z. are also grateful to DESY Directorate for the support in the framework of Moscow—DESY project on Monte-Carlo implementation for HERA—LHC.

References

- [1] J. Breitweg et al. (ZEUS Collaboration), Phys. Lett. **B 472**, 175 (2000).
- [2] A. Atkas et al. (H1 Collaboration), Eur. Phys. J. **C 38**, 437 (2005).

- [3] S. Chekanov et al. (ZEUS Collaboration), *Eur. Phys. J. C* **49**, 511 (2007).
- [4] F.D. Aaron et al. (H1 Collaboration), *Eur. Phys. J. C* **66**, 17 (2010).
- [5] M. Fontannaz, J.P. Guillet, G. Heinrich, *Eur. Phys. J. C* **21**, 303 (2001).
- [6] M. Fontannaz, G. Heinrich, *Eur. Phys. J. C* **34**, 191 (2004).
- [7] A. Zembrzuski, M. Krawczyk, hep-ph/0309308.
- [8] A.V. Lipatov, N.P. Zotov, *Phys. Rev. D* **72**, 054002 (2005).
- [9] A.V. Lipatov, N.P. Zotov, *Phys. Rev. D* **81**, 094027 (2010).
- [10] V.N. Gribov, E.M. Levin, M.G. Ryskin, *Phys. Rep.* **100**, 1 (1983).
- [11] S. Catani, M. Ciafaloni, F. Hautmann, *Nucl. Phys. B* **366**, 135 (1991).
- [12] J.C. Collins, R.K. Ellis, *Nucl. Phys. B* **360**, 3 (1991).
- [13] E.M. Levin, M.G. Ryskin, Yu.M. Shabelsky, A.G. Shuvaev, *Sov. J. Nucl. Phys.* **53**, 657 (1991).
- [14] E.A. Kuraev, L.N. Lipatov, V.S. Fadin, *Sov. Phys. JETP* **44**, 443 (1976); **45**, 199 (1977).
- [15] I.I. Balitsky, L.N. Lipatov, *Sov. J. Nucl. Phys.* **28**, 822 (1978).
- [16] B. Andersson et al. (Small- x Collaboration), *Eur. Phys. J. C* **25**, 77 (2002); J. Andersen et al. (Small- x Collaboration), *Eur. Phys. J. C* **35**, 67 (2004); *Eur. Phys. J. C* **48**, 67 (2006).
- [17] A. Iudin et al. (ZEUS Collaboration), talk given at DIS'2013.
- [18] A.V. Lipatov, M.A. Malyshev, N.P. Zotov, *JHEP* **1205**, 104 (2012).
- [19] V.M. Abazov et al. (D0 Collaboration), *Phys. Lett. B* **714**, 32 (2012); **719**, 354 (2013).
- [20] T. Aaltonen et al. (CDF Collaboration), arXiv:1303.6136[hep-ex].
- [21] T.P. Stavreva, J.F. Owens, *Phys. Rev. D* **79**, 054017 (2009).
- [22] M.A. Kimber, A.D. Martin, M.G. Ryskin, *Phys. Rev. D* **63**, 114027 (2001).
- [23] G. Watt, A.D. Martin, M.G. Ryskin, *Eur. Phys. J. C* **31**, 73 (2003).
- [24] J.A.M. Vermaseren, NIKHEF-00-023 (2000).
- [25] E.L. Berger, E. Braaten, R.D. Field, *Nucl. Phys. B* **239**, 52 (1984).
- [26] A.V. Lipatov, *JHEP* **1302**, 009 (2013).
- [27] A.D. Martin, W.J. Stirling, R.S. Thorne, G. Watt, *Eur. Phys. J. C* **63**, 189 (2009).
- [28] G.P. Lepage, *J. Comput. Phys.* **27**, 192 (1978).

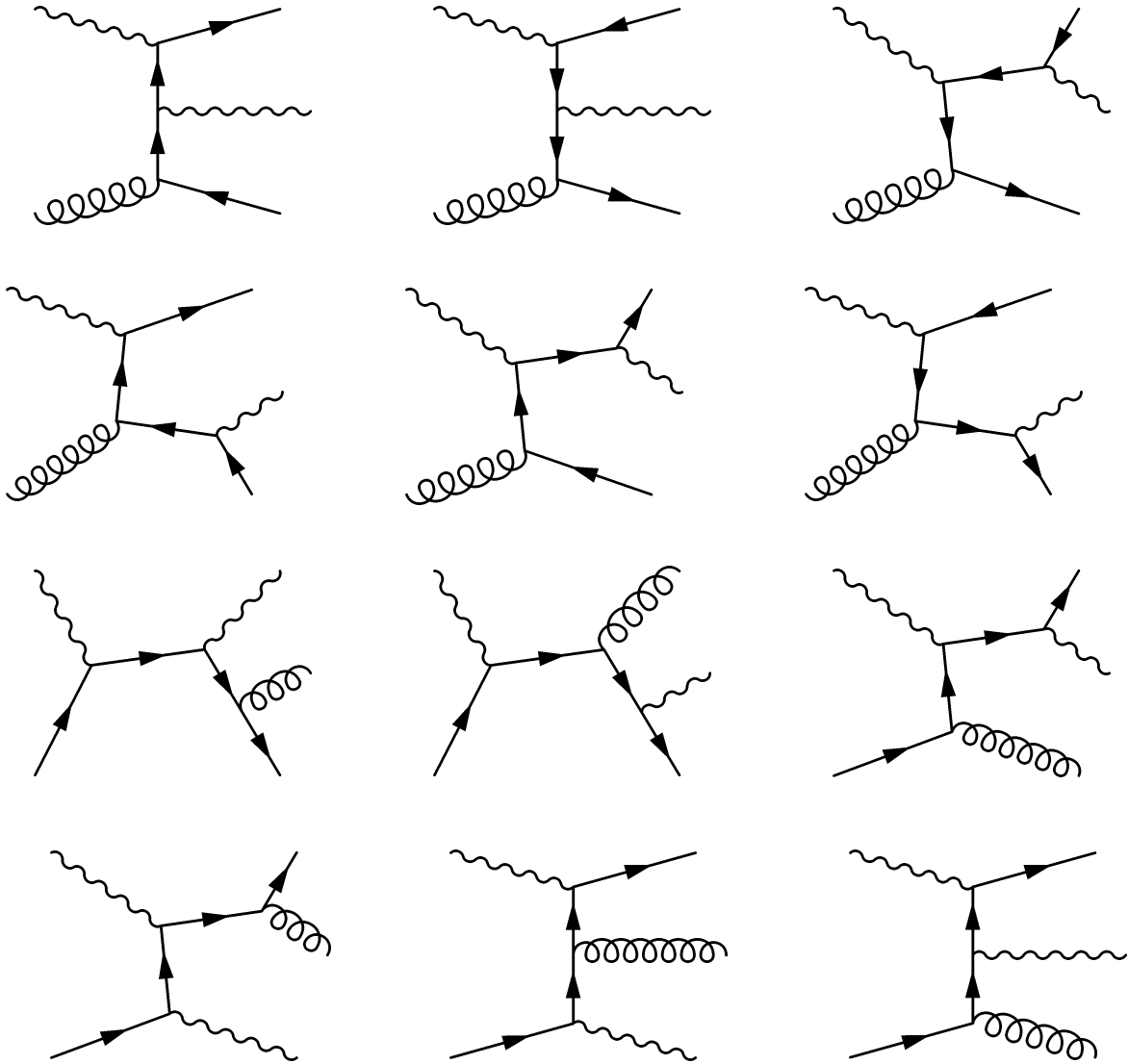


Figure 1: *The $2 \rightarrow 3$ diagrams considered*

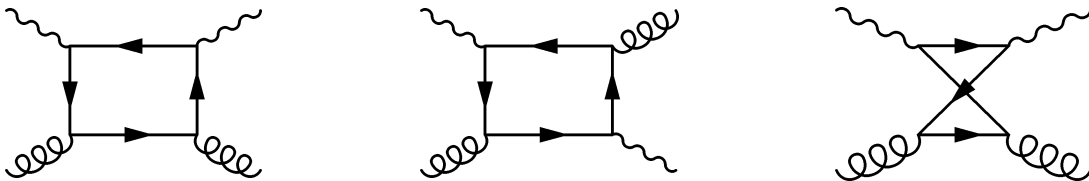


Figure 2: *The 'box'-diagrams. One should also take into account diagrams with the opposite direction of the fermion loop.*

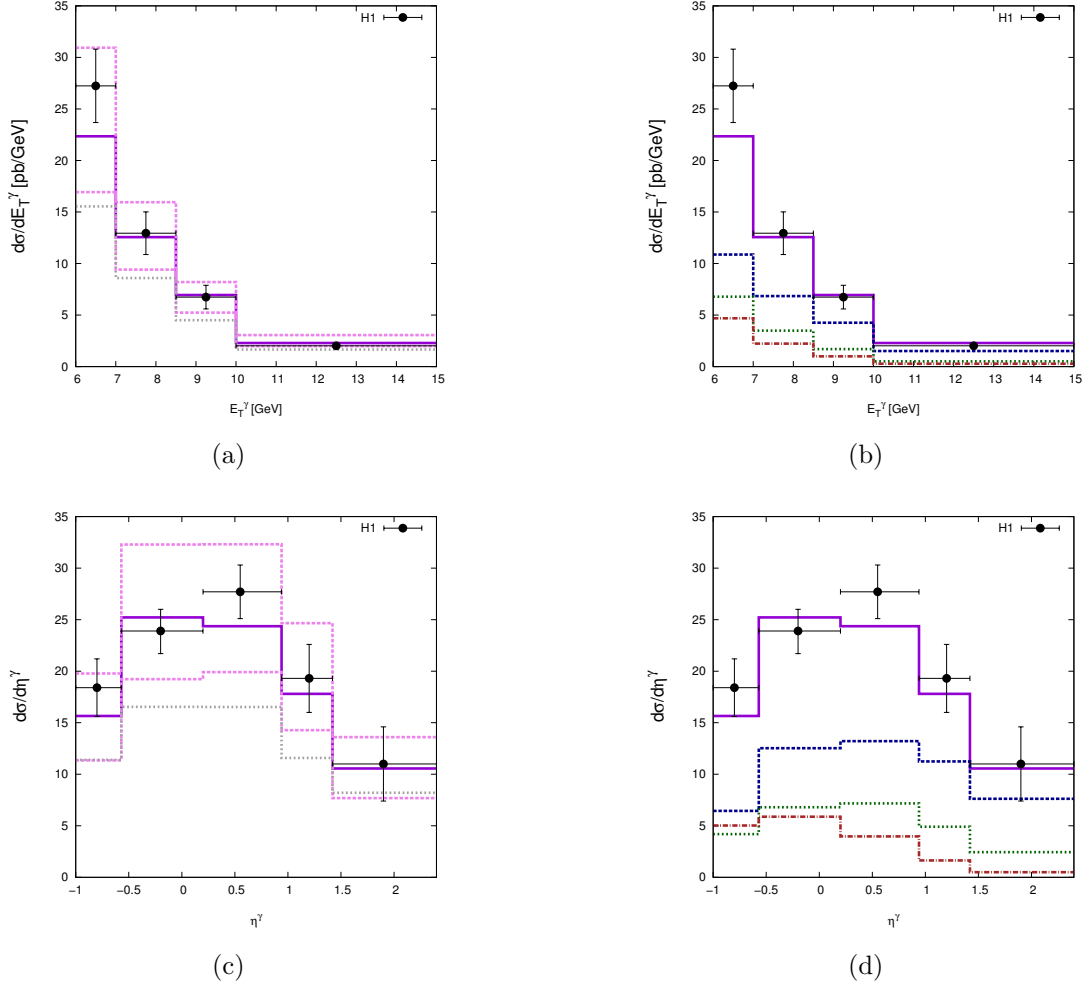


Figure 3: *The inclusive prompt photon photoproduction cross section as a function of photon transverse energy E_T^γ and pseudo-rapidity η^γ at HERA. The left panel: the solid curve corresponds to the KMR predictions at the default scale $\mu = E_T^\gamma$, whereas the upper and lower dashed curves correspond to scale variations described in the text; the dotted line represents the results obtained in previous papers [8, 9]. The right panel: the solid curve represents the total cross section; dashed, dotted and dash-dotted lines correspond to the contributions from $\gamma q \rightarrow \gamma g q$, $\gamma g \rightarrow \gamma q \bar{q}$ and $\gamma g \rightarrow \gamma g$ respectively. The experimental data are from H1 [4].*

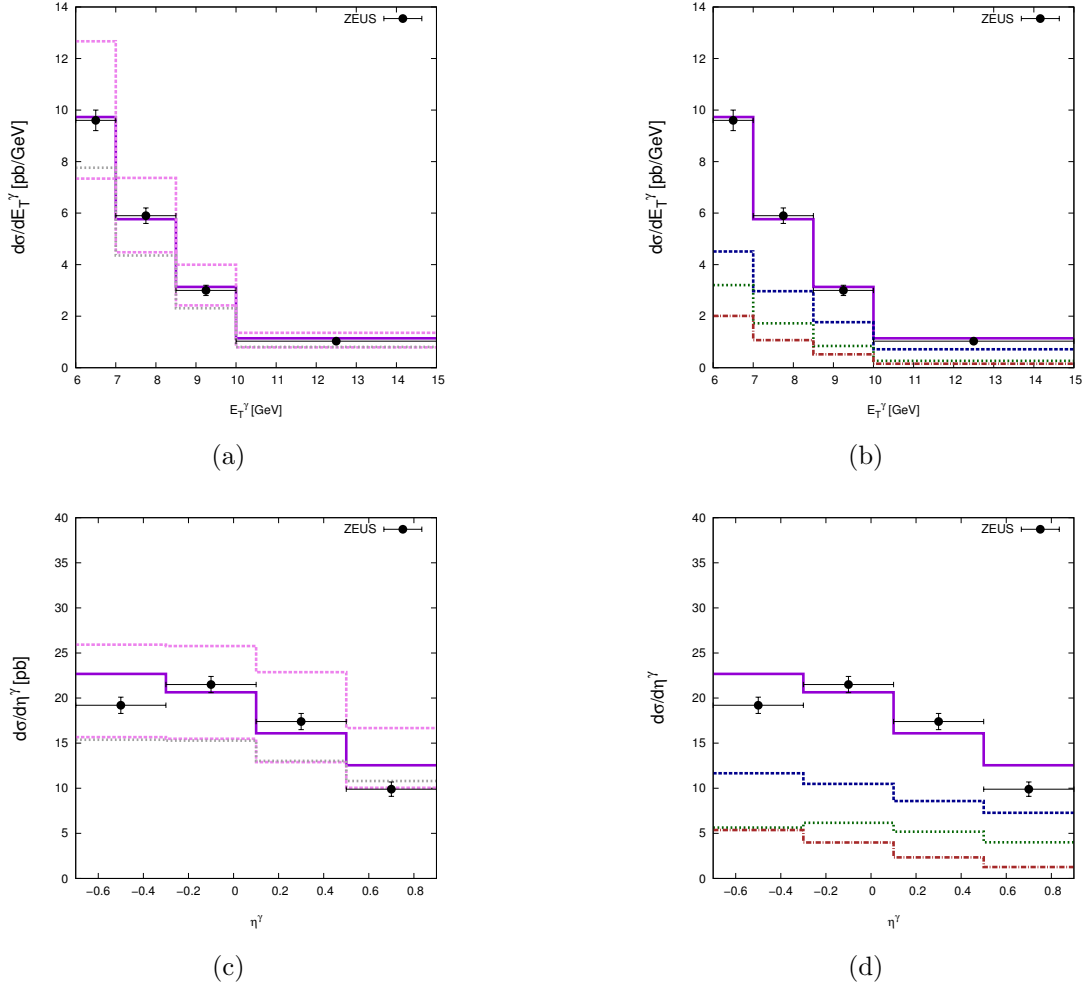


Figure 4: *The inclusive prompt photon photoproduction cross section as a function of photon transverse energy E_T^γ and pseudo-rapidity η^γ at HERA. The notations of the histograms are the same as in Fig. 3. The experimental data are from ZEUS [17].*

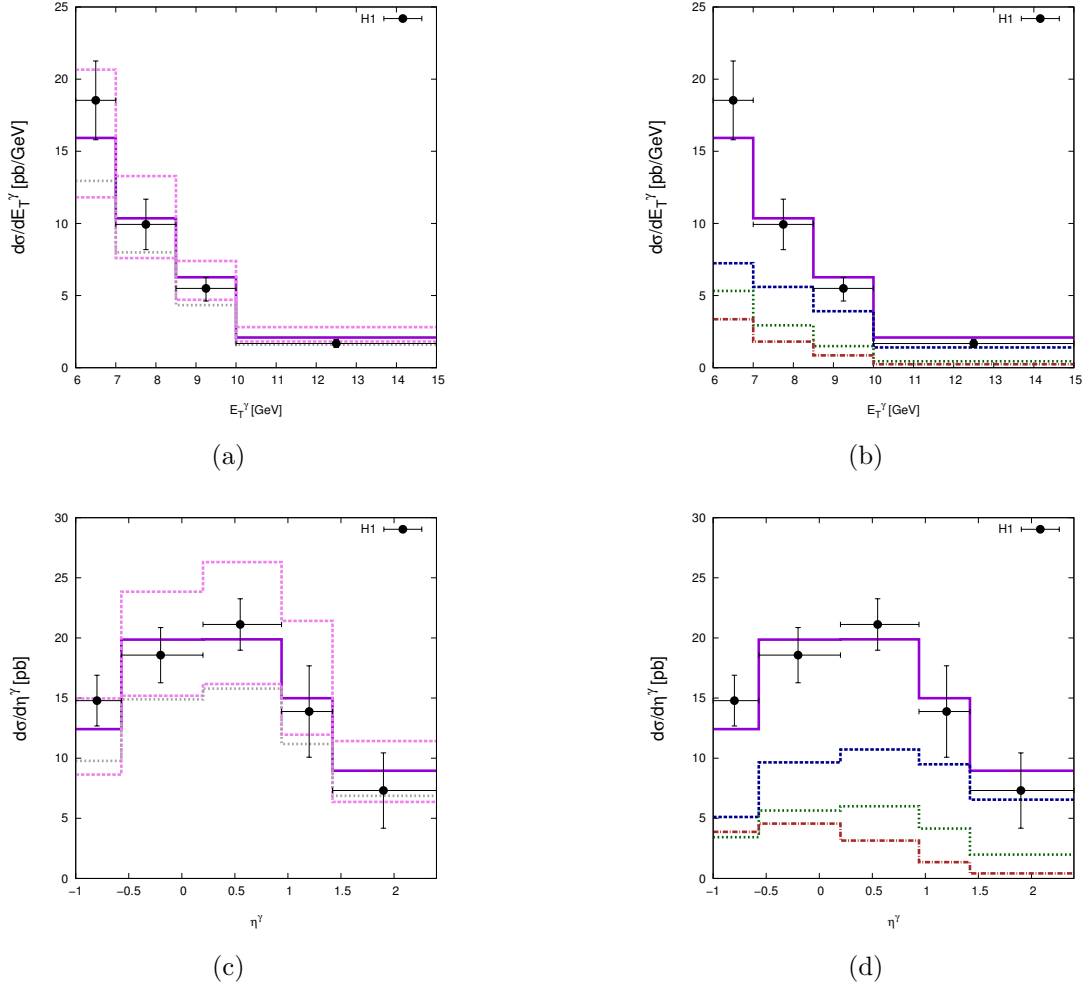


Figure 5: The associated with a jet prompt photon photoproduction cross section as a function of photon transverse energy E_T^γ and pseudo-rapidity η^γ at HERA. The notations of the histograms are the same as in Fig. 3. The experimental data are from H1 [4].

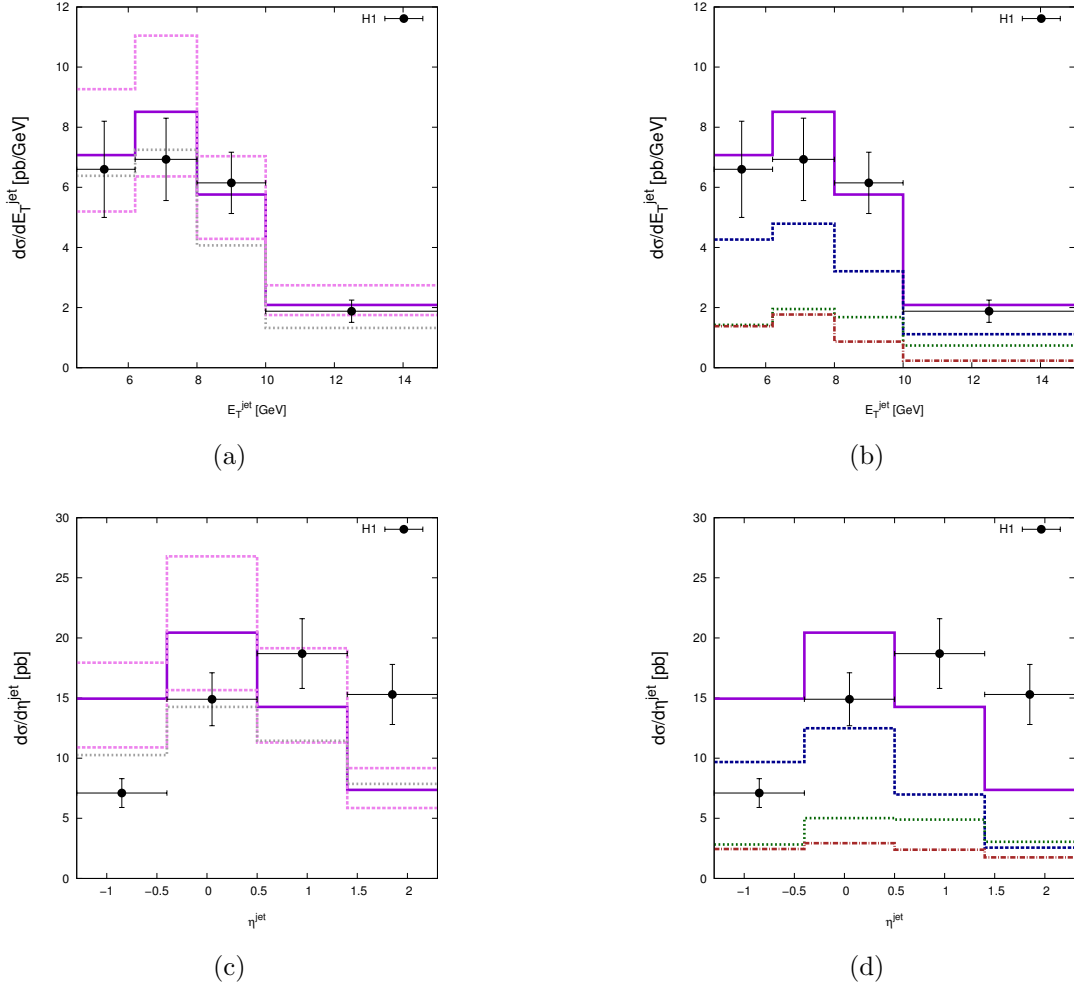


Figure 6: The associated with a jet prompt photon photoproduction cross section as a function of jet transverse energies E_T^{jet} and pseudo-rapidities η^{jet} at HERA. The notations of the histograms are the same as in Fig. 3. The experimental data are from H1 [4].

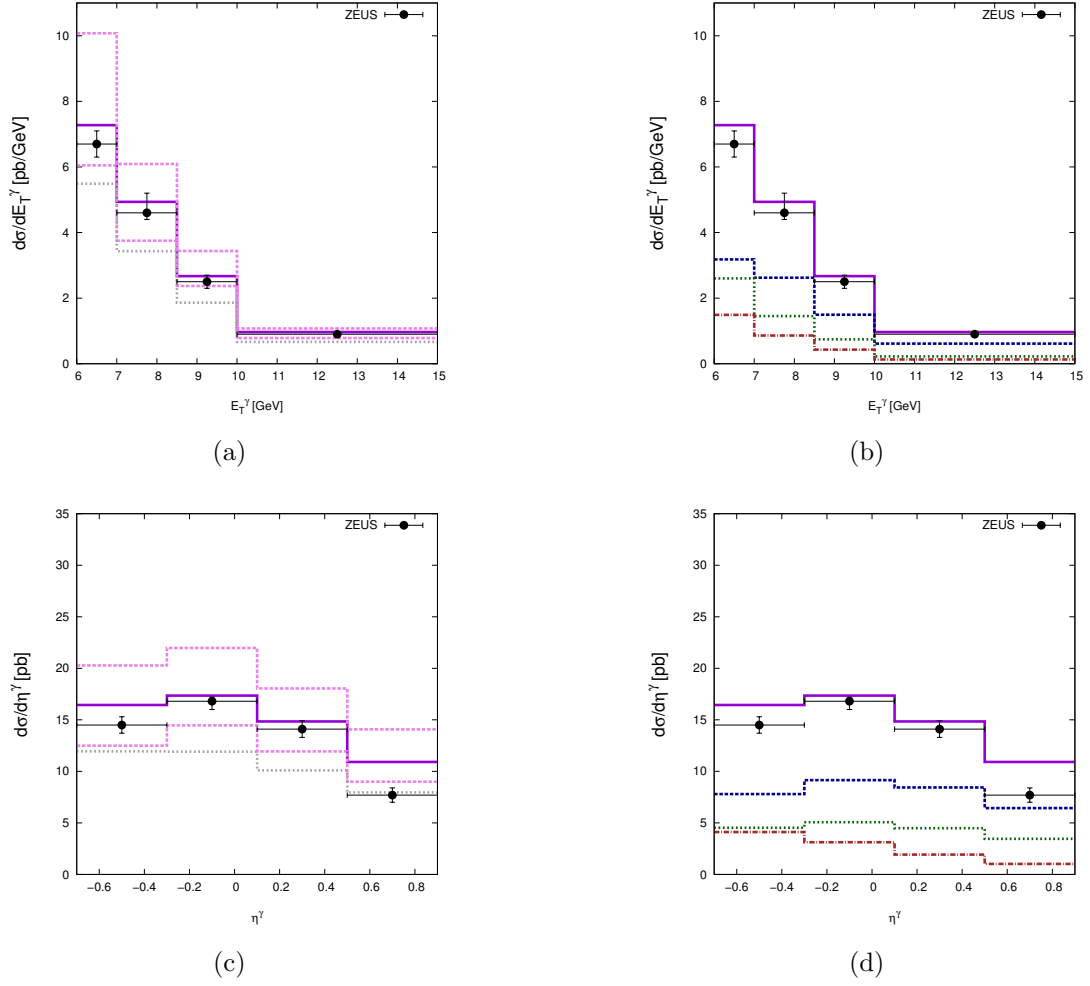


Figure 7: The associated with a jet prompt photon photoproduction cross section as a function of photon transverse energy E_T^γ and pseudo-rapidity η^γ at HERA. The notations of the histograms are the same as in Fig. 3. The experimental data are from ZEUS [17].

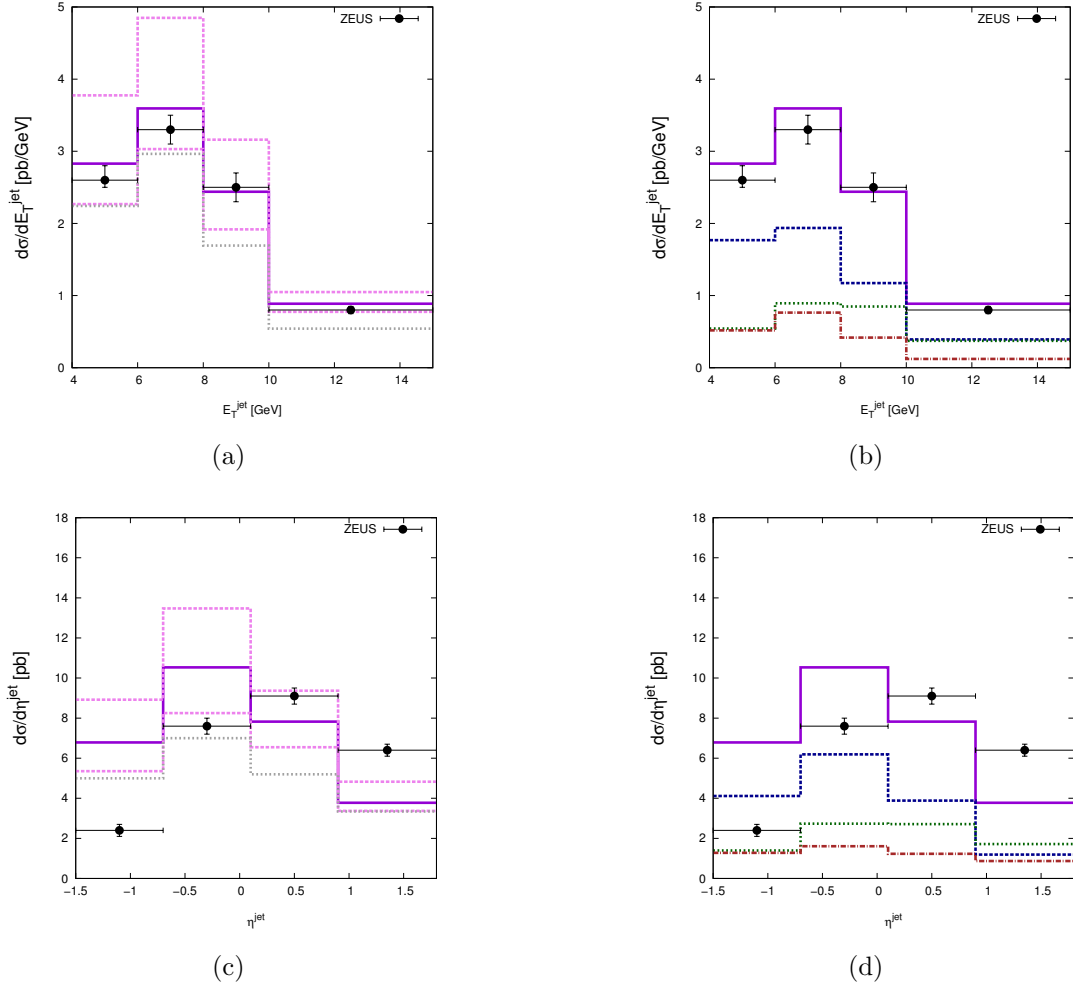


Figure 8: *The associated with a jet prompt photon photoproduction cross section as a function of jet transverse energies E_T^{jet} and pseudo-rapidities η^{jet} at HERA. The notations of the histograms are the same as in Fig. 3. The experimental data are from ZEUS [17].*

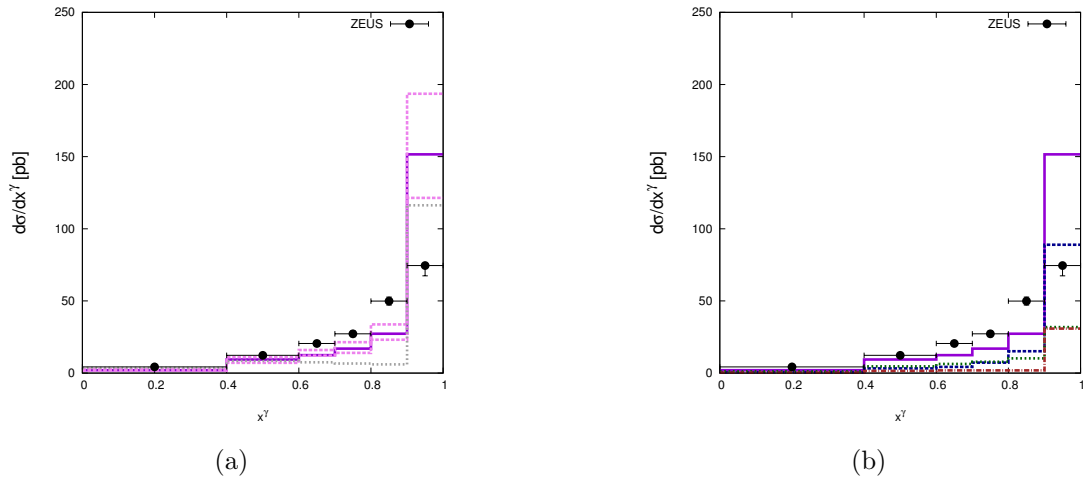
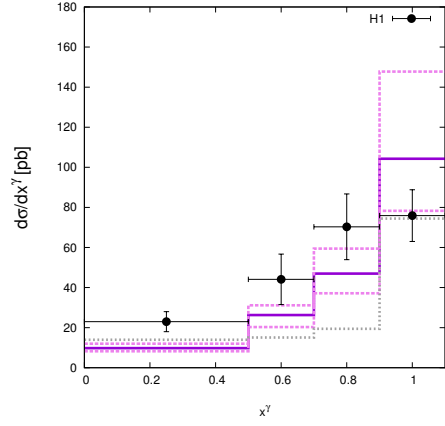
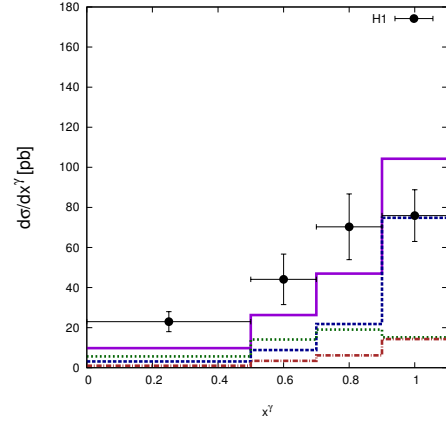


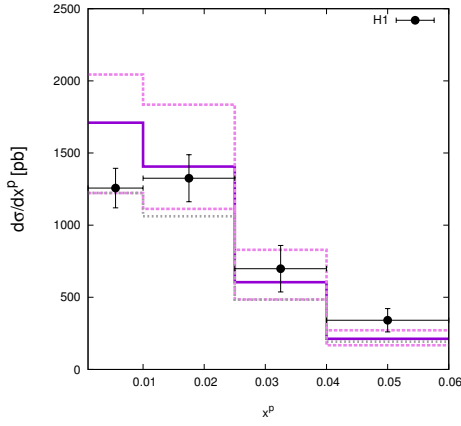
Figure 9: *The associated with a jet prompt photon photoproduction cross section as a function of the longitudinal momentum of a parton from the initial photon x_γ^{obs} at HERA. The notations of the histograms are the same as in Fig. 3. The experimental data are from ZEUS [17].*



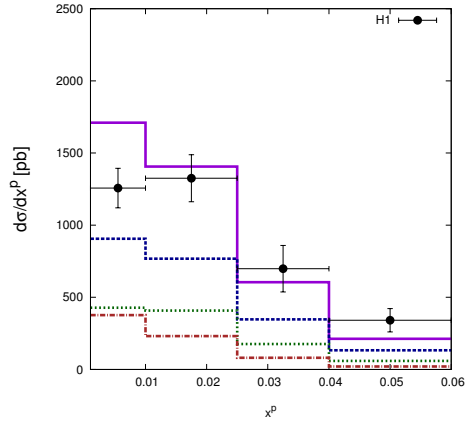
(a)



(b)



(c)



(d)

Figure 10: The associated with a jet prompt photon photoproduction cross section as a function of the x_γ^{LO} and x_p^{LO} variables at HERA. The notations of the histograms are the same as in Fig. 3. The experimental data are from H1 [4].